



## A hybrid strategy of lattice Boltzmann method and finite volume method for combined conduction and radiation in irregular geometry

Yujia Sun, Xiaobing Zhang\*

School of Energy and Power Engineering, Nanjing University of Science and Technology, Nanjing 210094, China



### ARTICLE INFO

#### Article history:

Received 27 October 2017

Received in revised form 13 January 2018

Accepted 15 January 2018

Available online 7 March 2018

### ABSTRACT

Lattice Boltzmann method (LBM) has been a trendy tool for fluid flow and heat transfer problems. Recently it has been applied to combined heat transfer problems with radiation, while most of the work consider a square enclosure. To extend the LBM to combined heat transfer problems with radiation in irregular geometries, it is coupled with the finite volume method (FVM) to solve the energy equation and radiative transfer equation (RTE), respectively. Blocked-off method is used in the FVM to approximate the curved boundary for radiation modeling. By using the half-way bounce back boundary method in the LBM, it can be perfectly coupled with the blocked-off FVM. Treatments of complex boundaries of these two methods are validated, and then the hybrid method is used to solve combined conduction and radiation heat transfer in enclosures with inclined and curved walls. Effects of the conduction-radiation number, optical thickness, scattering albedo and wall emissivity on the temperature distribution and wall heat flux are analyzed. Results show that this hybrid method can solve combined conduction and radiation heat transfer problems in irregular geometries.

© 2018 Elsevier Ltd. All rights reserved.

### 1. Introduction

Lattice Boltzmann method (LBM) is becoming a popular and useful computational tool for many areas, such as fluid flow, heat transfer and multiphase flow [1–16]. Because it is based on the mesoscopic kinetic equations, it has many attractive advantages, such as simple treatment of irregular geometries, high parallelism and simple coding procedure. Due to its high popularity, LBM has also been extended to multi-physics problems, such as combined heat transfer problems with radiation, in which LBM is coupled with various radiative transfer equation (RTE) solvers for combined conduction/convection and radiation problems, such as discrete ordinates method (DOM) [17,18], finite volume method (FVM) [19,20], control volume finite element method (CVFEM) [21], and also LBM [22,23]. However, most of the hybrid solvers consider a square or rectangular domain, and cannot deal with the cases with irregular geometries, where the LBM has intrinsic advantage over traditional methods. Additionally, combined conduction and radiation heat transfer problems in engineering applications usually involve irregular enclosures, treatment of complex boundaries in the hybrid solver is hence desirable and beneficial.

Usually unstructured mesh is used to discretize the domain in the framework of FVM, Finite Element method (FEM) to handle the irregular enclosure, such as in [24–31]. Bouzgarrou [24] extended the LBM to solve conduction-radiation problem in complex geometries using a general unstructured grid for the first time. The energy equation is solved by the Control Volume Lattice Boltzmann method and the RTE is solved by the Control Volume Finite Element method. This method is validated by various geometries with inclined wall and curved walls and have the advantage of obtaining smooth heat flux profiles along the complex boundaries. While our intent here is to extend the LBM to the combined conduction and radiation heat transfer in complex geometries in Cartesian grids. One way to achieve this goal is to use methods that do not need unstructured meshes to treat the complex boundaries, such as the spectral collocation method [32–36] and the meshless method [37–40]. Zhang [37,38] developed a natural element method for the combined conduction and radiation heat transfer in irregular geometries for two-dimensional and three-dimensional enclosures. Luo [40] coupled the LBM and the collocation meshless methods to a combined natural convection and radiation in an eccentric annulus, in which the meshless method share the lattice nodes in the LBM as the collocation points. Thus no additional grids or interpolation operations are required between these two solvers. It seems to the author that this is the only work that combines the LBM and a RTE solver to solve the combined heat transfer with radiation in irregular geometry with Cartesian grids.

\* Corresponding author.

E-mail addresses: [runtowhere@msn.cn](mailto:runtowhere@msn.cn) (Y. Sun), [zhangxb680504@163.com](mailto:zhangxb680504@163.com) (X. Zhang).

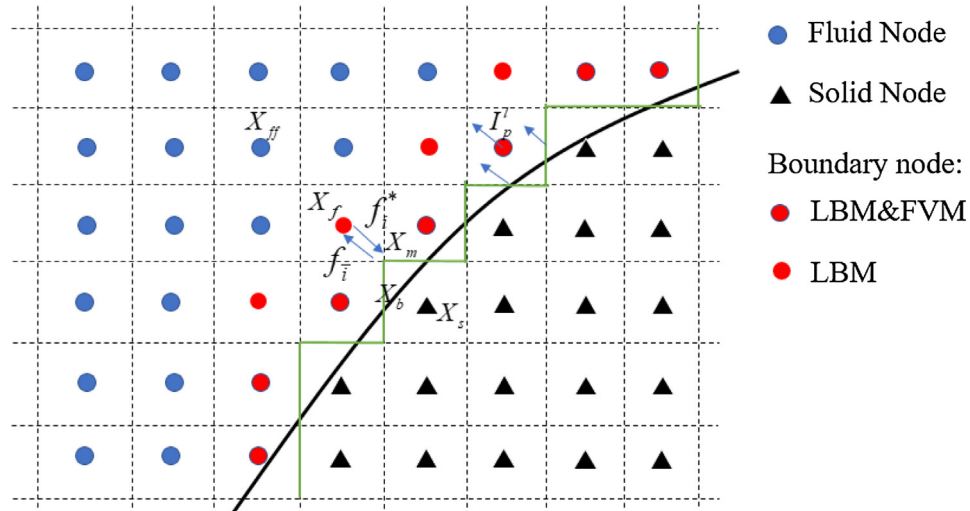


Fig. 1. Hybrid method for the LBM and the blocked-off FVM.

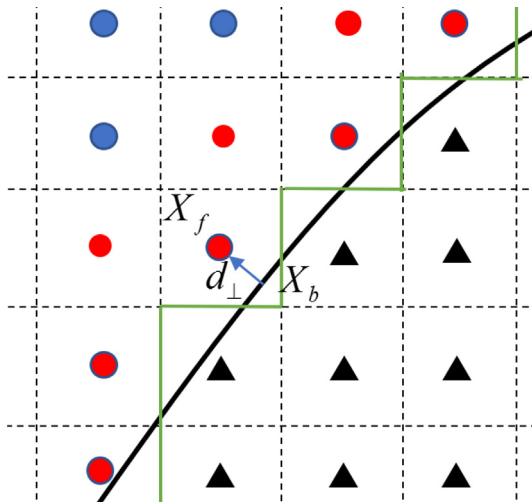


Fig. 2. Evaluation of heat flux on the complex boundary.

Considering that the DOM and FVM are the most widely used RTE solvers, it would be beneficial if only small changes to existing codes are required when one needs to couple them with the LBM for combined heat transfer problems. In the framework of FVM for Cartesian grids systems, there exists some methods to treat the complex boundaries, such as the body-fitted coordinates method, the blocked-off method, the embedded boundary treatments and the immersed boundary method. Among these methods, the blocked-off method is a potential method as it treats the boundary as a ladder grids like that in the LBM. Chai et al. [41] firstly applied the blocked-off method to radiation heat transfer for irregular geometries in Cartesian coordinates using the FVM. Byun [42] compared the multiblock, the blocked-off and the embedded boundary method for radiative heat transfer in a complex geometry using the FVM, and the performances of each method were highly satisfactory, although the blocked-off method produce some errors for the radiative heat flux. Aghajani and Abjadpour [43] compared the results of the blocked-off method, the embedded boundary method and unstructured meshes and obtained similar conclusions with Byun. The blocked-off method are also extended to three-dimensional radiation heat transfer

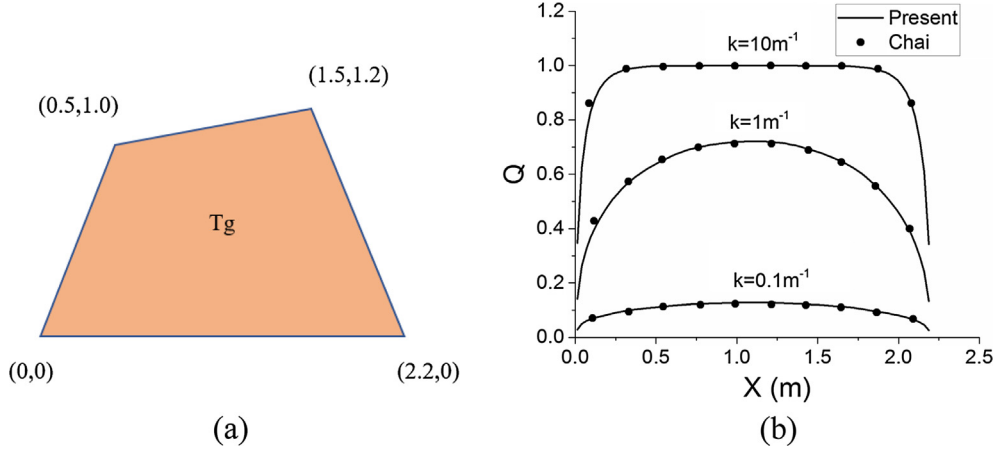
[44], collapsed dimension method [45], discrete transfer method [46]. Later on, Amiri et al. [47] developed a new form of blocked-off method and applied it to combined conduction and radiation heat transfer and then coupled it with a modified discrete ordinate method to eliminate the ray effect [48]. Effects of the conduction-radiation number, scattering albedo, extinction coefficient and asymmetry factor on the heat flux are analyzed. The authors proved that the blocked-off method can solve the combined conduction and radiation heat transfer in irregular geometries. Talukdar et al. [49,50] adopted the blocked-off method to the combined conduction and radiation in a porous media to calculate its effective thermal conductivity. More recently, Milad et al. [51] used the blocked-off and the embedded boundary method for combined conduction and radiation heat transfer. The results show that both methods have acceptable accuracies in terms of the temperature distribution and although the blocked-off method is less accurate, it needs much less computational time than the embedded boundary method.

From above literature reviews, the blocked-off method can deal with the complex boundaries in Cartesian grid systems. Because its similar approximation of complex boundary with LBM, it can be coupled with LBM naturally for combined heat transfer with radiation in irregular geometries. Whereas no report is found on this, to close this gap, this paper aims to implement this hybrid method to show its potential for combined conduction and radiation heat transfer problems in complex geometries. The remainder of this paper firstly gives the formulations of the LBM and FVM. Then the treatments of complex boundary of these two methods is presented, followed by corresponding validations, then the results and conclusions are given.

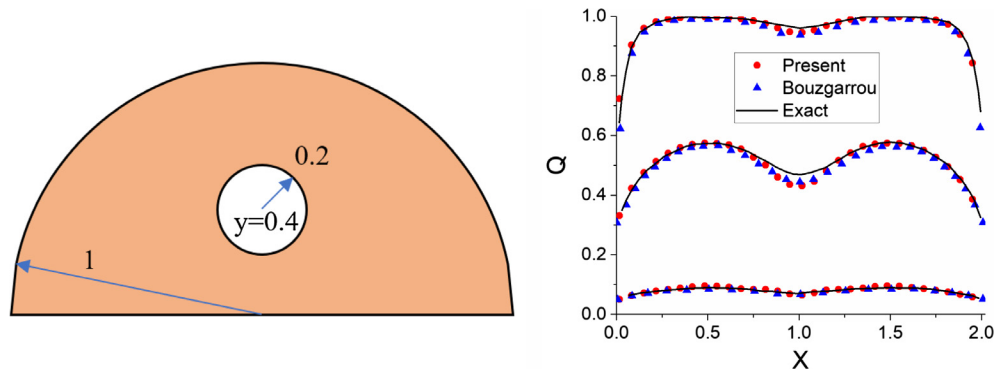
## 2. Mathematic formulations

### 2.1. The hybrid model

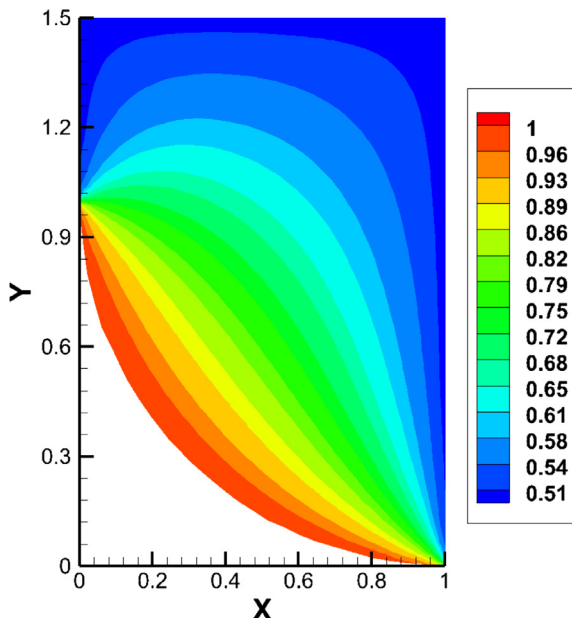
To demonstrate the hybrid solver for complex boundaries, Fig. 1 gives the grid systems used in the hybrid model with one curved boundary. In the LBM, the computational domain is discretized by structured mesh, and the curved boundary is approximated by ladder-like boundaries, as the green lines shown in the figure. Regions outside of the real objects are denoted as "Solid node",



**Fig. 3.** Quadrilateral enclosure: physical model and dimensionless flux on the bottom wall.

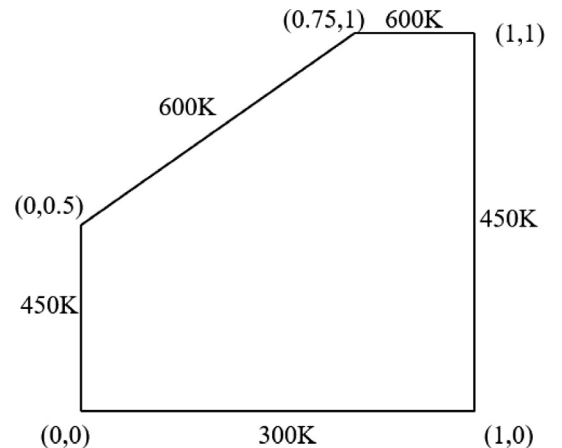


**Fig. 4.** Semi-circle: physical model and dimensionless flux on the bottom wall.



**Fig. 5.** Temperature at steady state for pure conduction case.

which are the black triangles in Fig. 1. While the “Fluid node” denotes the active regions needed to be solved by LBM. Any fluid nodes having a neighbor solid node needs special boundary treat-

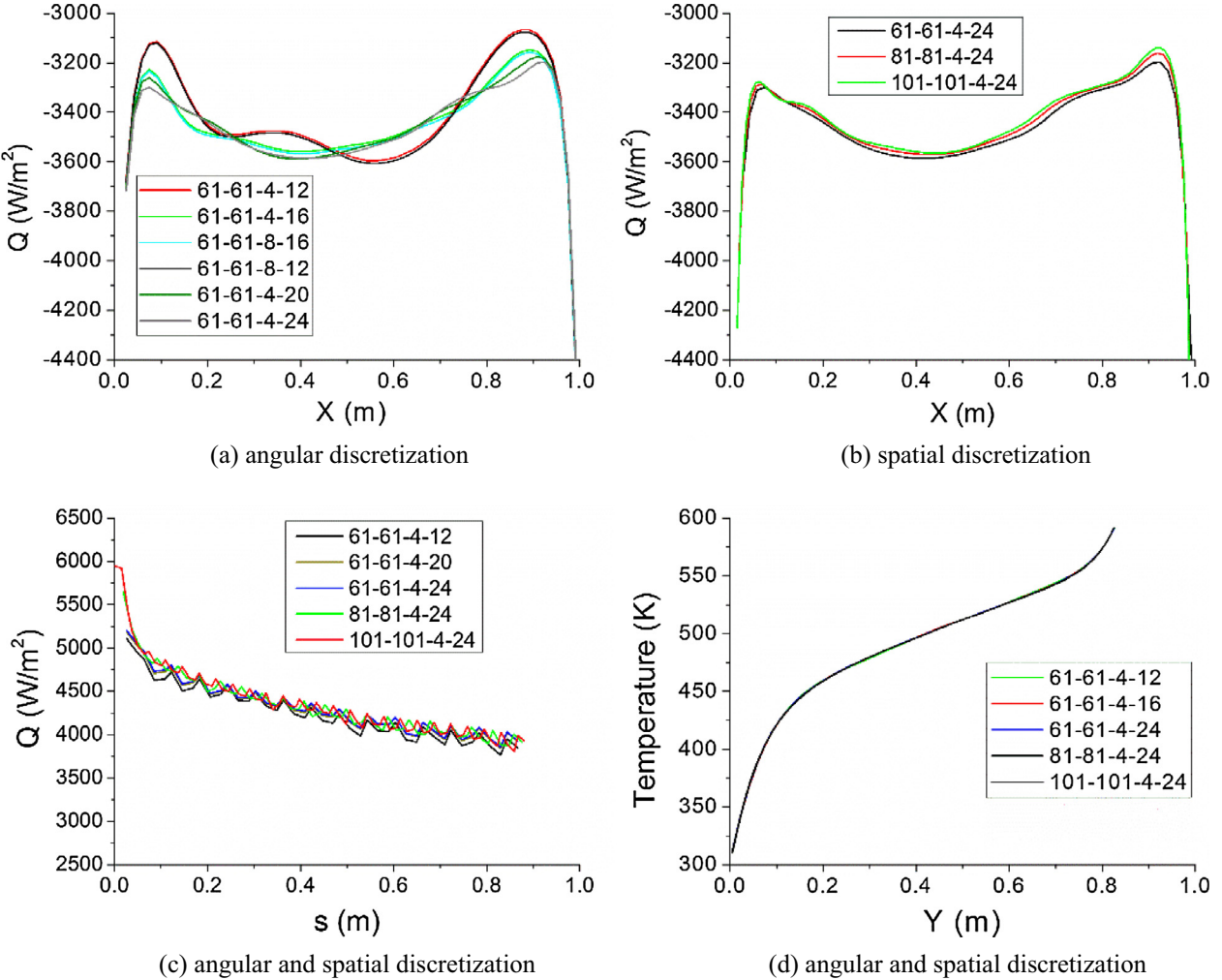


**Fig. 6.** Geometry of the trapezoidal enclosure.

ment in the LBM. While for the FVM solver, the blocked-off method is applied on the cells having intersections with the curbed boundary. The detailed boundary treatments for these two methods are given in the following sections.

## 2.2. Governing equations

Governing equation for the combined conduction and radiation heat transfer is as following:

Fig. 7. Grid dependent tests for case 1 for  $N = 0.01$ .

$$\rho c_p \frac{\partial T}{\partial t} = k \nabla^2 T - \nabla \cdot \mathbf{q}_r \quad (1)$$

where  $\rho$ ,  $c_p$  and  $k$  are the density, specific heat and thermal conductivity of the medium respectively and they are assumed to be constant in this work.  $\nabla \cdot \mathbf{q}_r$  is the divergence of the radiative heat source, which can be obtained by solving the RTE.

Relevant dimensionless numbers for this problem are conduction-radiation number and optical thickness:

$$N = \frac{kL}{\sigma T_{ref}^3} \quad (2)$$

$$\tau = \kappa L$$

where  $T_{ref}$  is the reference temperature and is taken as the hot temperature here,  $\sigma = 5.678 \text{ W}/(\text{m} \cdot \text{K}^4)$  is the Stefan-Boltzmann constant,  $k$  is the thermal conductivity,  $\kappa$  is the absorption coefficient and  $L$  is the length of the geometry. The conduction-radiation number denotes the relative influence of conduction and radiation to the energy transfer, and the smaller it is, the larger the contribution of radiation will be. The optical thickness affects the emission and absorbing behavior of the participating medium. Its order of magnitude has a direct effect on the radiative heat flux and radiative heat source. Both two quantities will influence the energy equation evolution if these exists thermal Neumann boundary condition. For Dirichlet boundary condition, as the case in this work, only radiative heat source will play a role in the temperature evolution.

### 2.3. FVM for RTE

The RTE for an absorbing and emitting gray medium is:

$$\frac{dl}{ds} = -(\kappa + \sigma)I + \kappa I_b + \frac{\sigma}{4\pi} \int_{\Omega'} Id\Omega' \quad (3)$$

where  $\kappa$  is the absorption coefficient,  $\sigma$  is the scattering coefficient. Integrating Eq. (3) over the solid angle and express it in Cartesian coordinate, we can obtain

$$\frac{\partial l^l}{\partial x} D_x^l + \frac{\partial l^l}{\partial y} D_y^l = -(\kappa + \sigma)l^l \Delta\Omega^l + \kappa I_b \Delta\Omega^l + \frac{\sigma}{4\pi} \int_{\Omega'} Id\Omega' \quad (4)$$

where  $D^l$  is given by

$$D^l = \int_{\Delta\Omega'} \mathbf{n} \cdot \mathbf{s}^l d\Omega \quad (5)$$

where  $\mathbf{n}$  is the unit vector in x or y direction.

Discretizing the physical domain into a finite number of control volumes and integrating above equation over these elements, the final radiation intensity formulation of one element can be written as:

$$I_p^l = \frac{D_x^l \Delta y l_e^l + D_y^l \Delta x l_s^l + (\kappa I_b + \frac{\sigma}{4\pi} G)_p \Delta x \Delta y \Delta \Omega^l}{D_x^l \Delta y + D_y^l \Delta x + (\kappa)_p \Delta x \Delta y \Delta \Omega^l} \quad (6)$$

After solving the above equation for all elements and angles, the radiative heat source is obtained by:

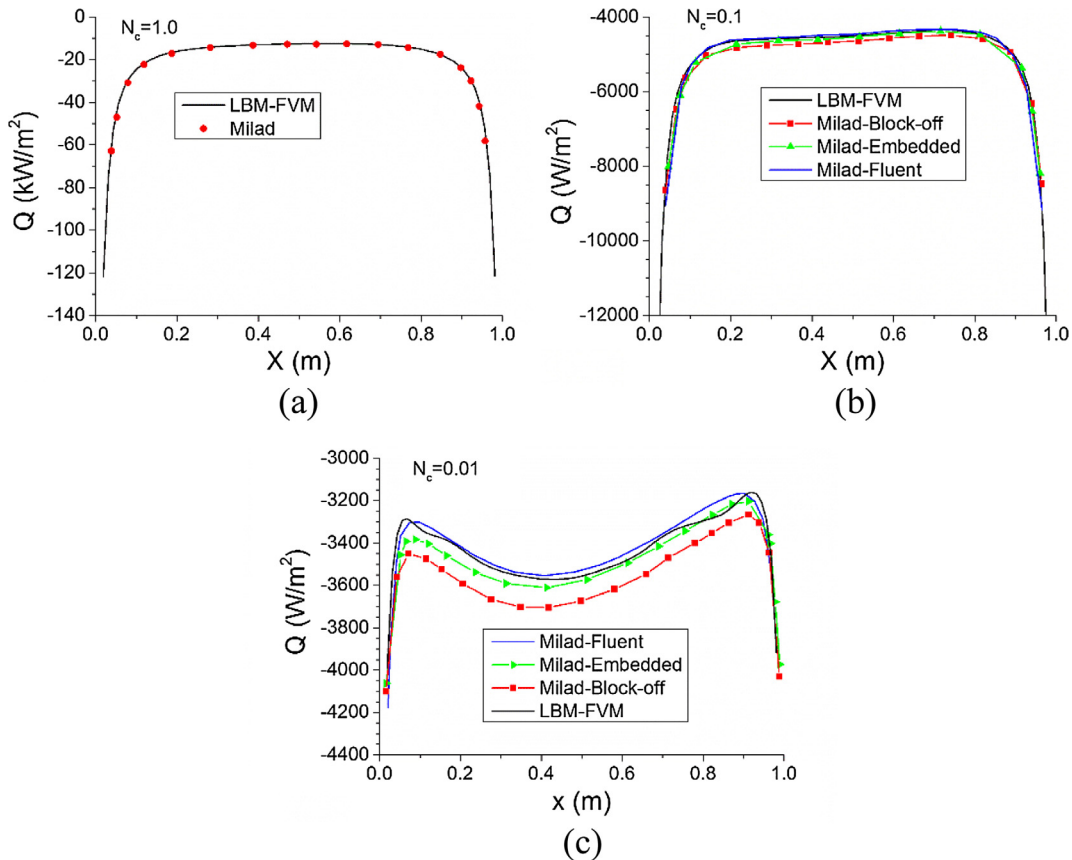


**Fig. 8.** Total heat flux along the bottom wall for three conduction-radiation number.

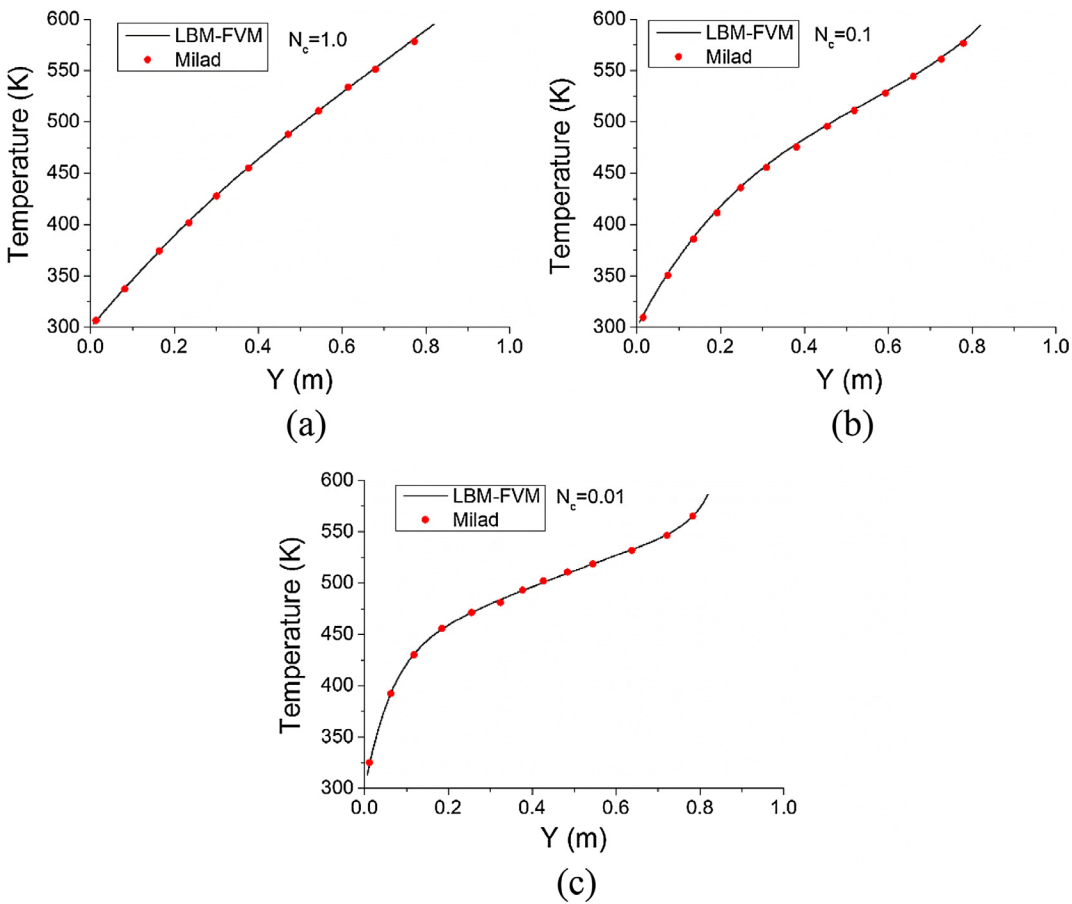


**Fig. 9.** Temperature distribution along the vertical center line.

$$\nabla \cdot \mathbf{q}_r = \kappa(4\pi I_b - G) \quad (7)$$

where  $G$  is the incident radiation:

$$G = \int_0^{4\pi} I d\Omega = \sum_l l^l \Delta\Omega^l \quad (8)$$

#### 2.4. Lattice Boltzmann method formulation

As no fluid flow is involved in current study, only one distribution function is used for the heat transfer in LBM,

$$g_i(r + e_i \Delta t, t + \Delta t) - g_i(r, t) = \frac{1}{\tau} (g_i^{eq}(r, t) - g_i(r, t)), \quad i = 0, 1, \dots, 8 \quad (9)$$

The macroscopic energy equation can be obtained from this equation by using Chapman-Enskog expansion, and D2Q9 model is used for the energy equation. The nine discrete velocities are given by

$$\mathbf{e}_i = \begin{cases} (0, 0) & i = 0 \\ \left(\cos \frac{(i-1)\pi}{2}, \sin \frac{(i-1)\pi}{2}\right) \frac{\delta x}{\delta t} & i = 1 - 4 \\ \left(\cos \frac{(i-1)\pi}{2}, \sin \frac{(i-1)\pi}{2}\right) \frac{\delta x}{\delta t} & i = 5 - 8 \end{cases} \quad (10)$$

where  $\delta x$  is the lattice grid unit and  $\delta t$  is the time step. The relaxation time  $\tau$  is related to the thermal diffusivity  $\alpha$  by

$$\alpha = c_s^2 \left( \tau - \frac{1}{2} \right) \delta t \quad (11)$$

The equilibrium energy distribution is

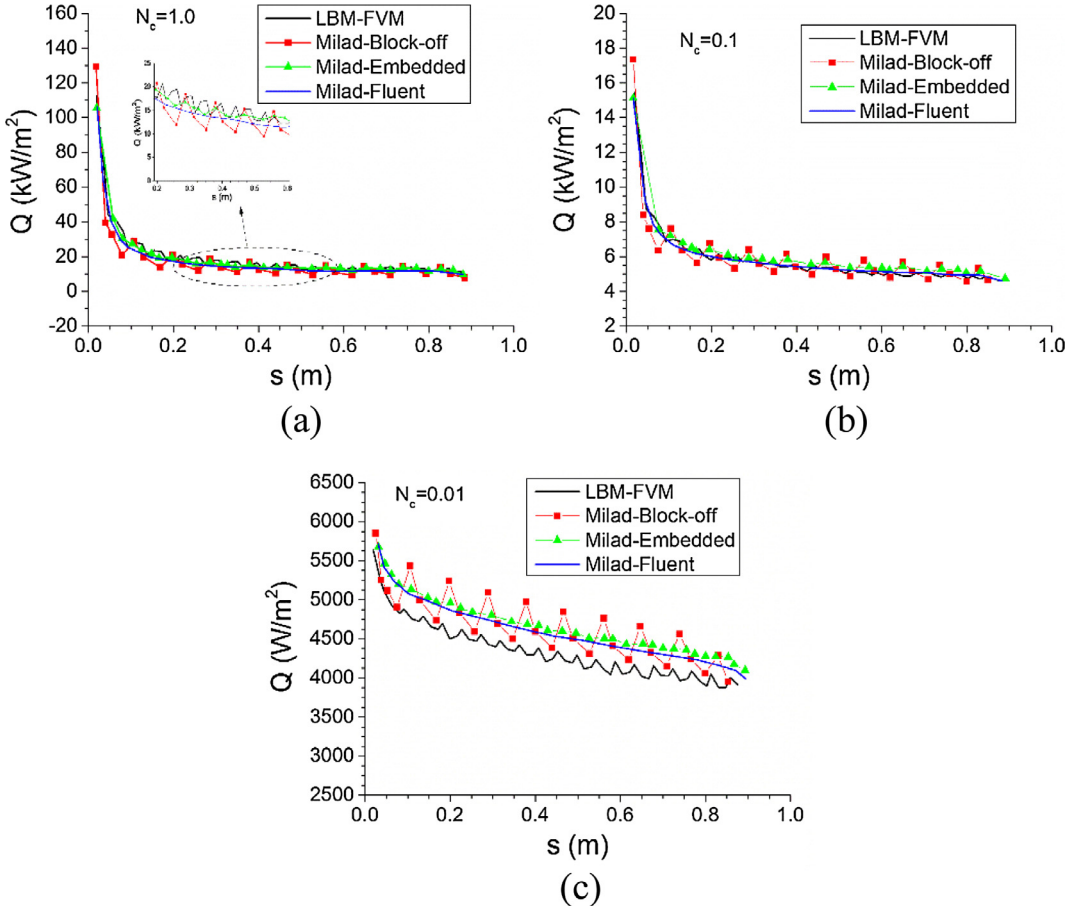


**Fig. 10.** Total heat flux along the inclined wall.

$$g_i^{eq} = \omega_i T \left( 1.0 + \frac{\mathbf{e}_i \cdot \mathbf{u}}{c_s^2} + \frac{(\mathbf{e}_i \cdot \mathbf{u})^2}{2c_s^4} - \frac{\mathbf{u} \cdot \mathbf{u}}{2c_s^2} \right) \quad (12)$$

where the lattice sound speed  $c_s = \sqrt{3} \delta x / \delta t$ , and the lattice weight factors are

$$\omega_i = \begin{cases} \frac{4}{9} & i = 0 \\ \frac{1}{9} & i = 1 - 4 \\ \frac{1}{36} & i = 5 - 8 \end{cases} \quad (13)$$

#### 2.5. Treatment of complex geometry for LBM

For the population distribution function of LBM near the boundary, as shown in Fig. 1, after the collision step at the fluid node  $X_f$ ,  $f_i^*$  leaves this fluid node and is bounced back at the middle point  $X_m$  and its direction is reversed with a modified magnitude following:

$$f_i = -f_i^* + 2\omega_i T_m \left[ 1 + \frac{(\mathbf{e}_i \cdot \mathbf{u}_m)^2}{2c_s^4} - \frac{\mathbf{u}_m \cdot \mathbf{u}_m}{2c_s^2} \right] \quad (14)$$

where  $T_m$  is the temperature at the middle point,  $\mathbf{u}_m$  is the velocity at the middle point. As the wall is stationary in this work, the terms involving velocity can be dropped. The middle point temperature can be calculated as:

$$T_m = \frac{\frac{1}{2}T_b + (\frac{1}{2} - \Delta)T_f}{1 - \Delta}, \quad \Delta \leqslant 1/2 \quad (15)$$

$$T_m = \frac{\frac{3}{2}T_b - (\Delta - \frac{1}{2})T_{ff}}{2 - \Delta}, \quad \Delta > 1/2 \quad (16)$$

**Fig. 10.** Total heat flux along the inclined wall.

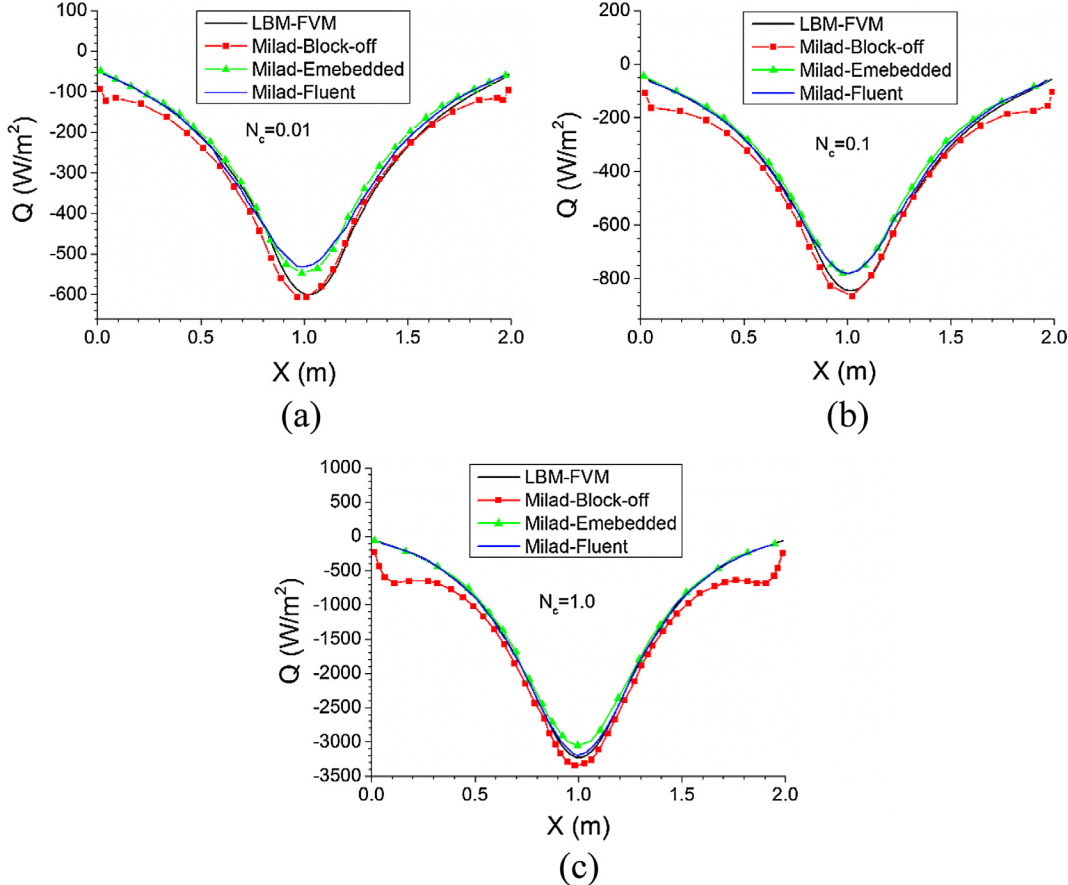


**Fig. 11.** Total heat flux along the bottom wall for the semicircular geometry: (a)  $N_c = 0.01$ , (b)  $N_c = 0.1$ , (c)  $N_c = 1.0$ .

where

$$\Delta = \frac{|X_s - X_b|}{|X_s - X_f|} \quad (17)$$

is the fraction of the boundary lattice link in the solid domain and it is in the range of 0–1. The middle point  $X_m$  maybe lies in either the fluid domain or the solid domain, depending on the value of this ratio.

## 2.6. Treatment of complex boundary for the FVM of RTE

The treatment of complex boundary for FVM of RTE is described for completeness. In the blocked-off method, the real complex boundary is approximated as ladder-like lines, as the green lines in Fig. 1. The blocked-off FVM shares the same inactive cells as in LBM and the RTE are not needed to be solved for these cells.

To account for the influence of the irregular geometries, an additional source term should be added to the radiation intensity formulation:

$$S = S_c + S_p I_p^m \quad (18)$$

Then the intensity equation become:

$$I_p^l = \frac{D_x^l \Delta y I_e^l + D_y^l \Delta x I_s^l + [(\kappa I_b)_p - S_c] \Delta x \Delta y \Delta \Omega^l}{D_x^l \Delta y + D_y^l \Delta x + [(\kappa)_p - S_p] \Delta x \Delta y \Delta \Omega^l} \quad (19)$$

The coefficients  $S_p$  and  $S_c$  are given appropriate values to the active cells those adjacent to inactive cells and zero for other active cells. For a black boundary, the additional source terms for cell A in Fig. 1 are

$$S_c = \frac{\Delta y}{\Delta x \Delta y \Delta \Omega^l} D_x^l I_b \quad S_p = 0.0 \quad (20)$$

Thus the intensity at the active cell near the boundary is

$$\begin{aligned} I_p^l &= \frac{D_x^l \Delta y I_e^l + D_y^l \Delta x I_s^l + (\kappa I_b)_p \Delta x \Delta y \Delta \Omega^l + D_x^l \Delta y I_b}{D_x^l \Delta y + D_y^l \Delta x + \kappa_p \Delta x \Delta y \Delta \Omega^l} \\ &= \frac{D_x^l \Delta y \times 0 + D_y^l \Delta x \times 0 + (\kappa I_b)_p \Delta x \Delta y \Delta \Omega^l + D_x^l \Delta y I_b}{D_x^l \Delta y + D_y^l \Delta x + \kappa_p \Delta x \Delta y \Delta \Omega^l} \\ &= \frac{(\kappa I_b)_p \Delta x \Delta y \Delta \Omega^l + D_x^l \Delta y I_b + D_y^l \Delta y I_b}{D_x^l \Delta y + D_y^l \Delta x + \kappa_p \Delta x \Delta y \Delta \Omega^l} \end{aligned} \quad (21)$$

The effect of desired boundary condition can now be captured by this corrected nodal radiation intensity. This practice enables solving radiative heat transfer in Cartesian coordinates with complex geometries, which makes it perfectly coupled with the LBM for combined heat transfer with radiation. Fine grid may be needed to reduce the errors caused by approximations of the actual curved boundary.

## 2.7. Evaluation of total heat flux along the complex boundaries

In the results sections, the total heat flux along the inclined or curved wall needs determination to evaluate the performance of the LBM-FVM.

The evaluation of heat flux along the complex boundary needs more steps than the straight boundary. Although the complex boundary is approximated as stair like grids, the determination of heat flux is based on the real boundary in this work (see

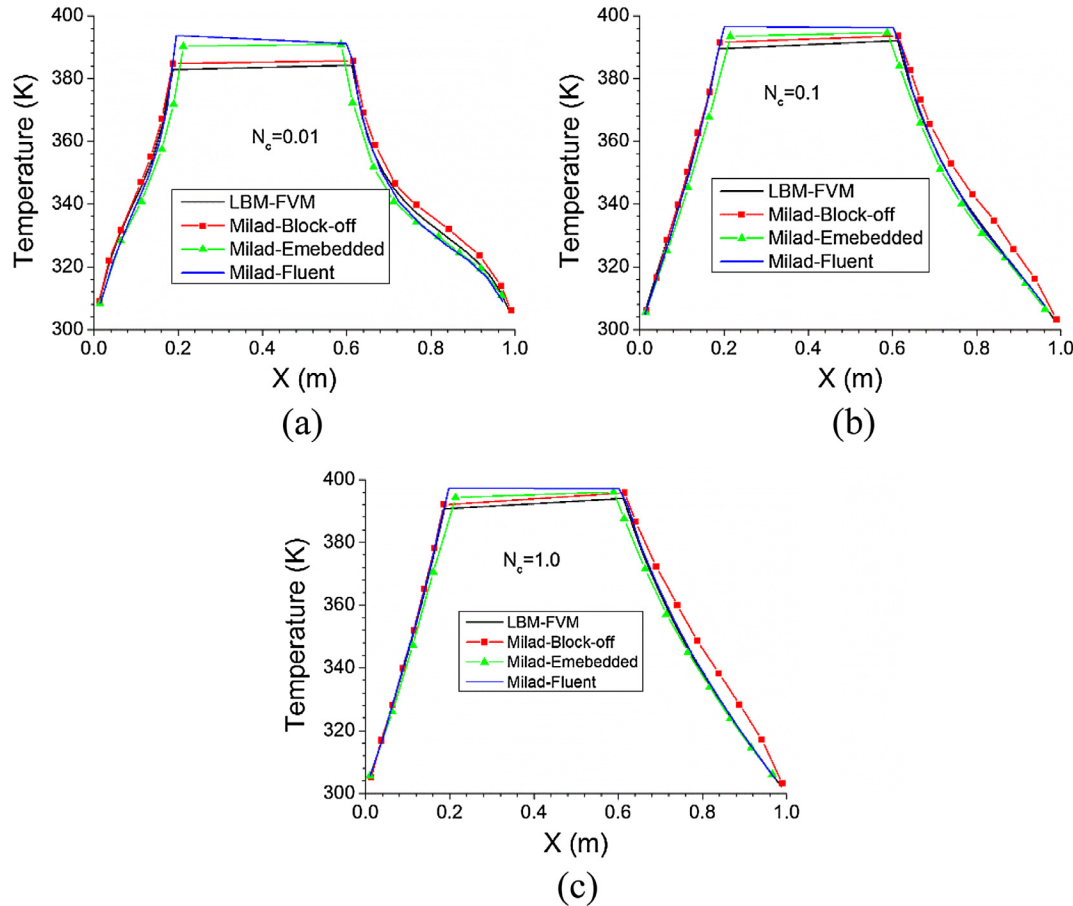


**Fig. 12.** Temperature along the vertical center line for the semicircular geometry: (a)  $N_c = 0.01$ , (b)  $N_c = 0.1$ , (c)  $N_c = 1.0$ .

Fig. 2). To achieve this goal, the distance,  $d_{\perp}$ , between the node  $X_f$  and the real boundary is obtained from geometrical information, and the cross point  $X_b$  is also determined. The conductive heat flux can then be calculated from:

$$q_c = -k \frac{\partial T}{\partial n} = -k \frac{T_f - T_w}{d_{\perp}} \quad (22)$$

The radiative heat flux along the real boundary is determined from this way that the radiation intensities along the boundary is approximated from node  $X_f$ , which is the similar to the straight wall with step scheme.

$$q_r = \sum_l D_{cn}^l I^l \quad (23)$$

where

$$D_{cn}^l = n_x D_x^l + n_y D_y^l \quad (24)$$

where  $n_x$  and  $n_y$  are the x and y component of wall normal direction.

### 3. Results and discussions

#### 3.1. Validations of blocked-off FVM

To ensure the correctness of the computational model, treatments of complex geometry of the FVM are firstly validated. The grid numbers are 101 in x and y direction, and 8 in polar direction and 16 in azimuthal direction.

Fig. 3(a) shows an irregular quadrilateral enclosure, and the medium is absorbing and emitting with temperature equals to

$T_g$ , whose absolute value is not important here since non-dimensional heat flux will be presented. The walls are black and 0 K. Dimensionless heat flux along the bottom wall for three absorption coefficients, namely, 0.1, 1, and  $10 \text{ m}^{-1}$  are plotted as Fig. 3(b). As can be seen, current results are in good agreement with Chai [41].

The accuracy of the blocked-off FVM is also validated for a case with curved wall, and the semi-circle benchmark problem is chosen for comparison, which is shown in Fig. 4. The medium is absorbing and emitting with a constant temperature of 1000 K and the walls are cold and black. The dimensionless radiative heat flux for three values of absorption coefficient along the bottom wall is also shown in Fig. 4. It can be seen that present results are in good agreement with those of Bouzgarrou [24] and the exact results.

#### 3.2. Validation of LBM for pure conduction in complex geometry

Before applying the LBM and blocked-off FVM to the combined conduction and radiation heat transfer in complex geometries, the LBM is validated for a pure conduction problem in a rectangle with a curved wall. The initial temperature in the domain is 0.5 and the curved wall is suddenly raised to 1.0 and the other walls are kept at 0.5. This grid size is 80 in x direction and 121 in y direction. The problem is investigated in Bouzgarrou [24]. The temperature at steady state is shown in Fig. 5, and it is in good agreement with that of Bouzgarrou [24], which is not shown here.

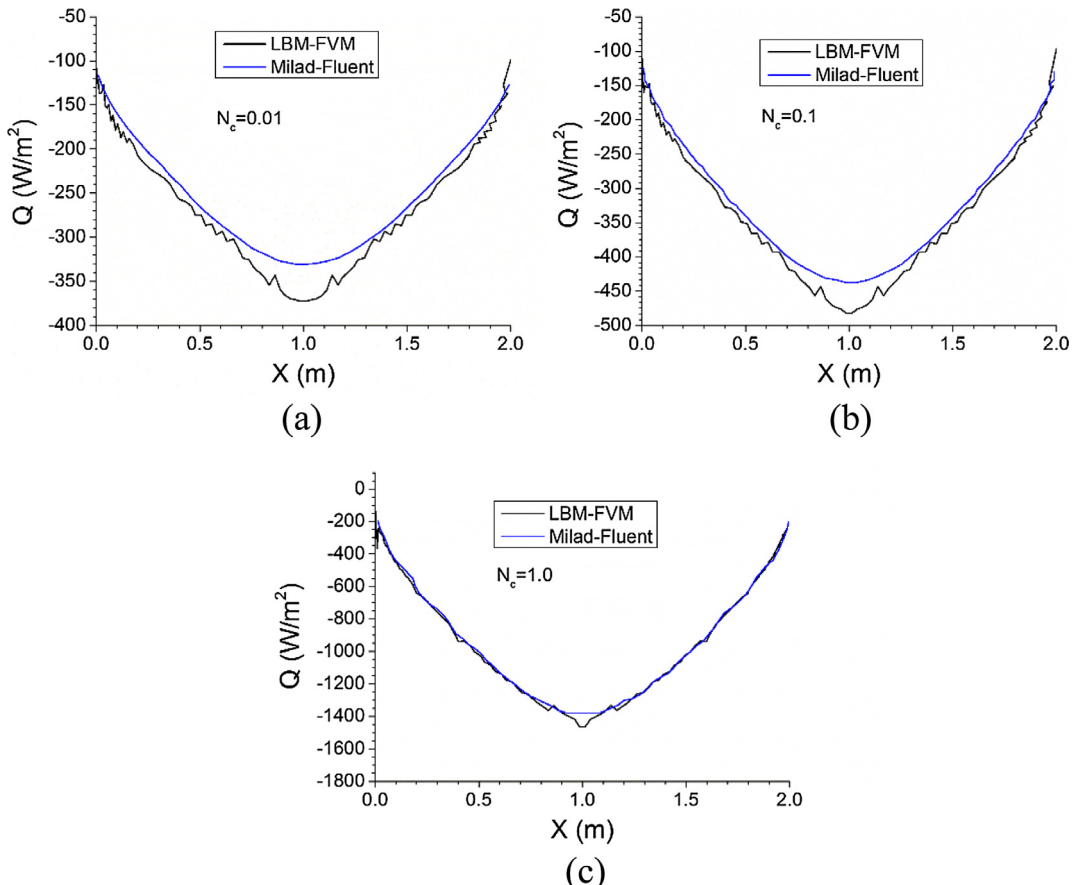


**Fig. 13.** Total heat flux along the outer circular wall for the semicircular geometry: (a)  $N_c = 0.01$ , (b)  $N_c = 0.1$ , (c)  $N_c = 1.0$ .

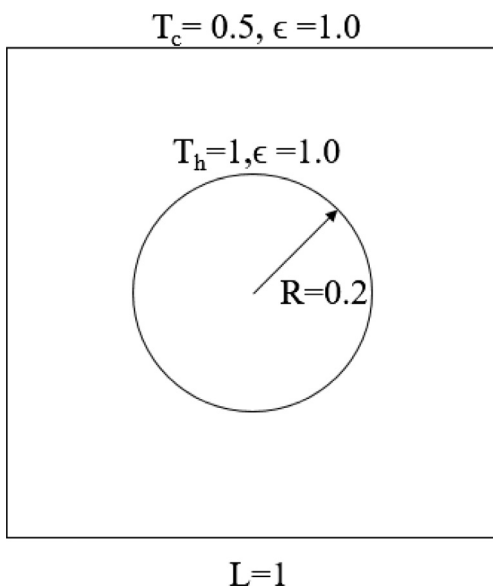


**Fig. 14.** Square enclosure with one circular wall.

### 3.3. LBM-FVM for a trapezoidal enclosure

This case is a combined conduction and radiation heat transfer problems in a trapezoidal enclosure with one inclined wall, as shown in Fig. 6. This case is investigated by Milad

[51] for evaluation of the performance of the embedded boundary method for the coupled conduction and radiation heat transfer.

Firstly, grid dependent tests are performed to study how the solution will vary with the grid number. After this, comparisons of heat flux along the straight wall, the inclined wall and the temperature profile with existing paper are presented to show the performance of the current LBM-FVM for combined conduction and radiation heat transfer.

Fig. 7(a) and (b) shows the effect of spatial and angular discretizations on the total heat flux along the bottom wall. The four numbers in the legend indicate the control volume size in the  $x$ ,  $y$ , polar and azimuthal directions, respectively. It can be seen that the total heat flux depends more on the azimuthal grid number than the polar grids number and spatial grid number. Fig. 7(c) and (d) shows the effect of both the angular and spatial discretization on the total heat flux along the inclined wall and the temperature along the vertical center line of the domain, respectively. The temperature is not sensitive to the grid number, while the total heat flux along the inclined wall has obvious dependence on the grid number. The heat flux profile is oscillating because the inclined wall is approximated as stair-step walls in the blocked-off FVM, and it's an intrinsic drawback of this method. From these figures, the configuration of 81-81-4-24 can yield acceptable grid independent results and is used for further validations of this case with existing paper. For larger conduction-radiation number, the conduction heat transfer will become more dominating and the effect of angular discretization will be smaller, so the grid dependent tests are not performed for these cases.

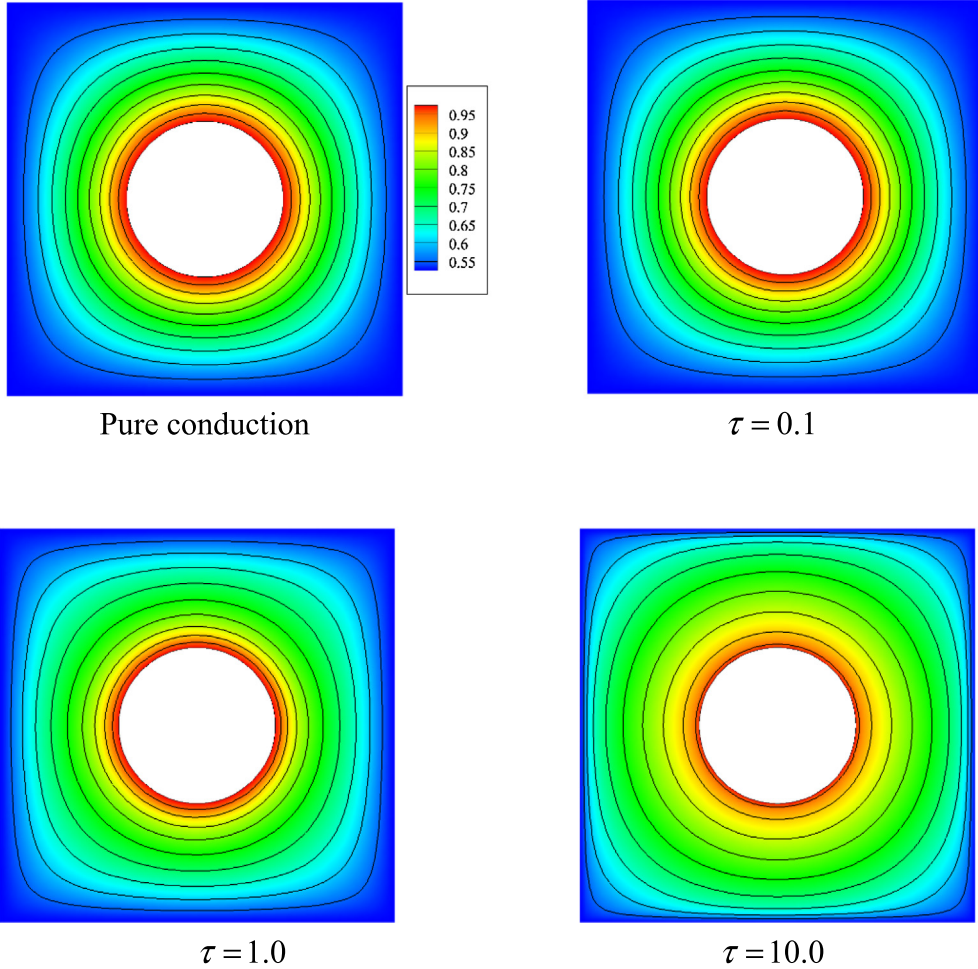


**Fig. 15.** Temperature contours for pure conduction and different optical thickness for  $N = 0.01$ .

**Fig. 8** shows the total heat flux along the bottom wall for the trapezoidal enclosure for different conduction-radiation numbers. For the case with  $N = 0.01$ , the radiation heat transfer dominates over the conduction heat transfer and the heat flux profiles shows non-linear behavior. The result of present LBM-FVM is very close to that of Fluent and better than embedded boundary method and the blocked-off method in Milad. This may be due to the fact that present study uses more grids than Milad.

**Fig. 9** shows the temperature distribution along the vertical center line for the trapezoidal enclosure for different conduction-radiation numbers. As results of three method in Milad are almost the same, only one reference is presented here. As shown in this figure, results of present LBM-FVM are in great agreements with those of Milad, and thus validates the capabilities if the hybrid method of LBM and blocked-off FVM for the temperature predictions.

**Fig. 10** shows the total heat flux along the inclined wall for the trapezoidal enclosure for different conduction-radiation number. As this inclined wall is approximated as step-like grids in the blocked-off method, the heat flux obtained will show oscillatory behavior. For  $N = 0.01$ , the present LBM-FVM under-predicts the wall heat flux while with smaller amplitude than the blocked-off in Milad. The embedded boundary method performs well for this case. When the  $N$  increases, the oscillating behavior become less obvious for the present LBM-FVM and the results are in good agreement with those of embedded boundary method and Fluent.

### 3.4. LBM-FVM for a semicircular enclosure with inner circle

This case has the same semicircle geometry as the benchmark validation case used in Section 3.1. The initial temperature of the domain is 300 K, and the temperature of the inner circle is raised to 400 K after  $t > 0$ . This case is proposed and investigated by Milad [51] to evaluate the performances of the blocked-off method and the embedded boundary method in complex geometries for coupled conduction and radiation heat transfer. It differs from the trapezoidal enclosure case that this geometry includes curved boundary and blockage effect from inner circle and thus poses more challenges for the blocked-off method. The grid for this case is 81 nodes in x dimension, 41 nodes in y dimension and 4–24 in angular dimension, which is the same as in the trapezoidal enclosure case.

**Fig. 11** shows the total heat flux along the bottom wall for the semicircular geometry for different conduction-radiation number. Comparisons with results of Milad are presented. The blocked-off method of Milad has somewhat large errors near the boundaries, while the present LBM blocked-off FVM performs very well near the boundaries without an oscillating pattern. Compared to the embedded boundary method, the blocked-off method has larger discrepancies in the center point and present LBM-FVM method has better accuracies than the original blocked-off method, especially for the case with  $N = 1.0$ .

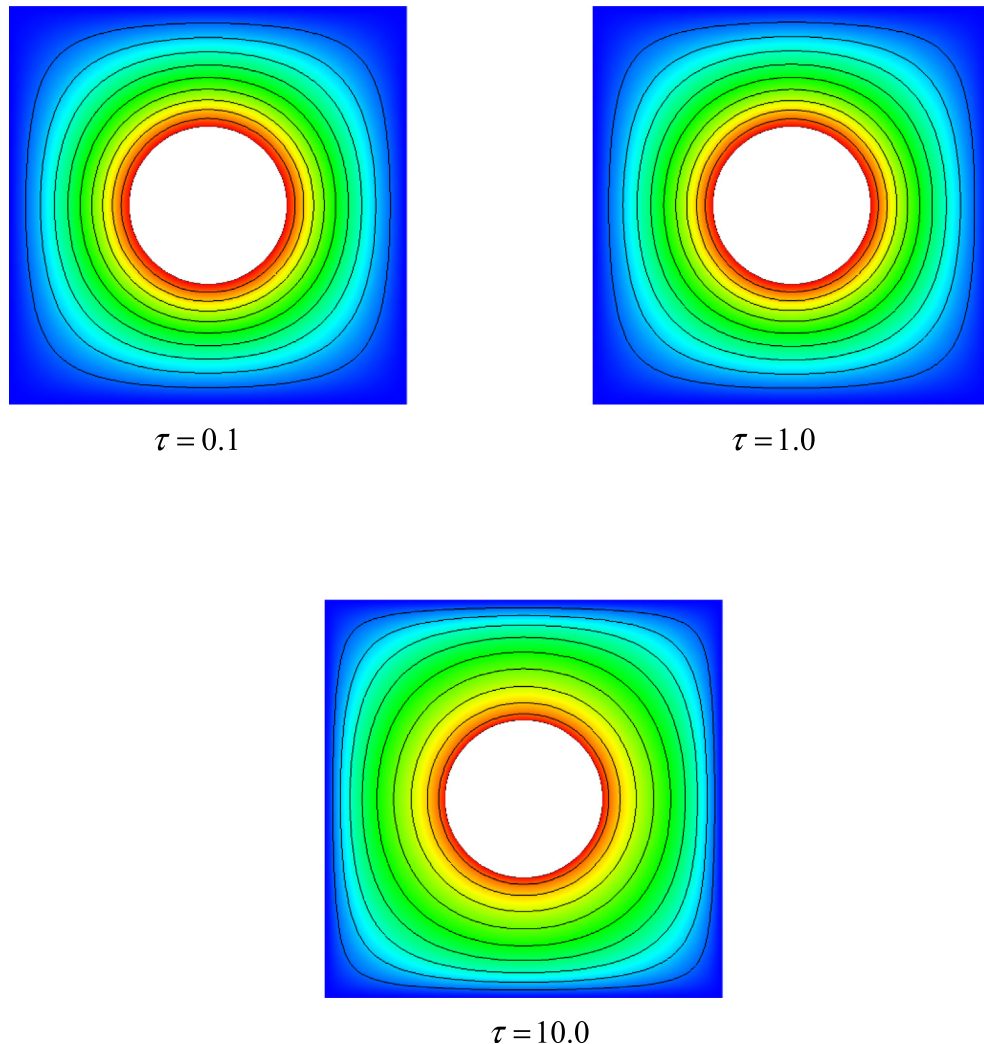


**Fig. 16.** Temperatures contours for different optical thickness for  $N = 0.1$ .

In conclusion, present LBM-FVM is acceptable for the evaluation of the total heat flux along the bottom wall, and its accuracy increases with the increase of conduction-radiation number.

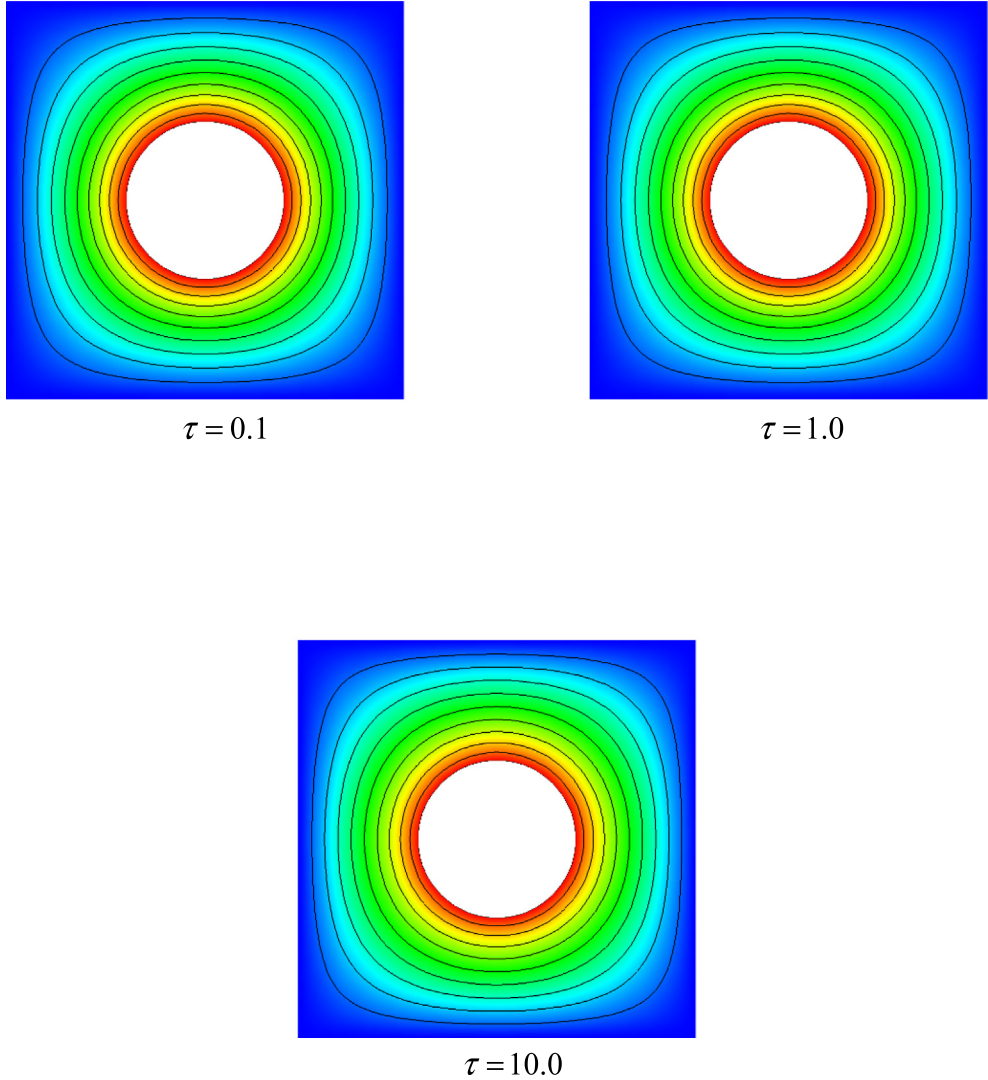
Fig. 12 shows the temperature profile along the vertical center line for the semicircular geometry for different conduction-radiation numbers. It is to be noted that the horizontal lines in these figures are not real temperature profiles as there is no medium in the inner circle. They are shown in the figures due to plot issues. It can be seen from these figures that the embedded boundary method tends to under-predict the temperature and the blocked-off method of Milad over-predict the temperature, especially in the upper part. The present LBM-FVM also over-predict the temperature for the case with  $N = 0.01$ , but with better accuracy than the blocked-off method of Milad. With the increase of the conduction-radiation number, results of LBM-FVM are almost identical to those of Fluent. This improved accuracy of present LBM-FVM is maybe due to refined treatment of the complex boundaries of LBM for the conduction heat transfer.

Fig. 13 shows the total heat flux along the outer circular wall for the semicircular geometry for different conduction-radiation number. Heat flux along the curved boundary is difficult to obtain as the boundary is modeled by step-like grids, and blocked-off results are not presented in Milad. While this paper develops a way to cal-

culate the heat flux along the curved wall through Eq. (23). Results of embedded boundary method were given but with large disturbances, and are not presented here. Only results of Fluent from Milad are plotted here for comparisons. One big difference between present LBM-FVM and the embedded boundary method is their accuracy dependence on the conduction-radiation number. The embedded boundary method has better accuracy for smaller  $N$  values, while present LBM-FVM has better accuracy for larger  $N$  values. For small  $N$  value, the total heat flux is in the range of 100–400 W/m<sup>2</sup>, and result of LBM-FVM shows oscillating behavior. When the  $N$  increases, the total heat flux gets larger and the discrepancies between LBM-FVM and Fluent are smaller. From these analyses, the LBM-FVM can capture the qualitative behavior of the heat flux along the curved wall, although with maximum error about 15% near the center point of the curved wall for the radiation dominated case.

### 3.5. Square enclosure with one circular wall

In this section, we apply the validated LBM-FVM to a combined conduction and radiation heat transfer in a square with an internal circle obstacle. The inner wall is at high temperature  $T_h = 1$ , and the outer wall is at cold temperature  $T_c = 0.5$ . The medium is absorbing and emitting with initial temperature of 0.5. The ratio



**Fig. 17.** Temperatures contours for different optical thickness for  $N = 1.0$ .

of the diameter of the inner circle to the length of the square is 0.4, as shown in Fig. 14. The grid numbers are 101 in x and y direction, and 8 in polar direction and 16 in azimuthal direction.

### 3.5.1. Steady state temperature distribution

Fig. 15 shows the steady temperature contours for  $N = 0.01$  for three optical thickness,  $\tau = 0.1, 1.0, 10.0$ . 9 isotherms from 0.55 to 0.95 with interval 0.05 are shown in each figure. For pure conduction condition, heat is transferred outwards due to temperature gradient. For small optical thickness, as the absorption is small, the resulting radiative heat source is also small compared to the diffusion term. In this case, the conduction heat transfer dominates over the radiation transfer, leading to similar temperature contours with pure conduction condition. With the increase of the optical thickness, temperature becomes more uniform in the medium. Isotherms of 0.55 and 0.95 are very close to outer wall and inner wall respectively for  $\tau = 10.0$ . The reason for isotherm of 0.95 being closer to the inner wall compared to cases with smaller optical thickness is that large optical thickness hinders the radiation heat transfer. This large temperature difference near the boundary is

similar to that of the radiation equilibrium condition, in which there exists a temperature slip. While conduction still plays a role here, although it is very small, temperature is continuous near the boundaries. The interaction of radiation and conduction for this configuration is the same to other geometries [20], and this proves that the LBM-FVM is able to solve the combined problems in complex geometries.

Figs. 16 and 17 show the temperature contours for different optical thicknesses for  $N = 0.1$  and  $1.0$  respectively. Similar to the case of  $N = 0.01$ , with the increase of the optical thickness, the temperature is more uniform in the medium, except the regions close to the hot inner wall. For isotherm of 0.95, its distance to the inner wall is very small for  $N = 0.01$  and  $\tau = 10.0$ , and this distance increases when optical thickness decreases. While for larger conduction-radiation number, this dependence on the optical thickness is becoming smaller. For the same optical thickness, the temperature decreases with the increase of the conduction-radiation number. This is because radiation becomes less important for larger  $N$  and conduction dominates over radiation. When  $N = 1.0$ , the temperature field is almost not affected by the optical

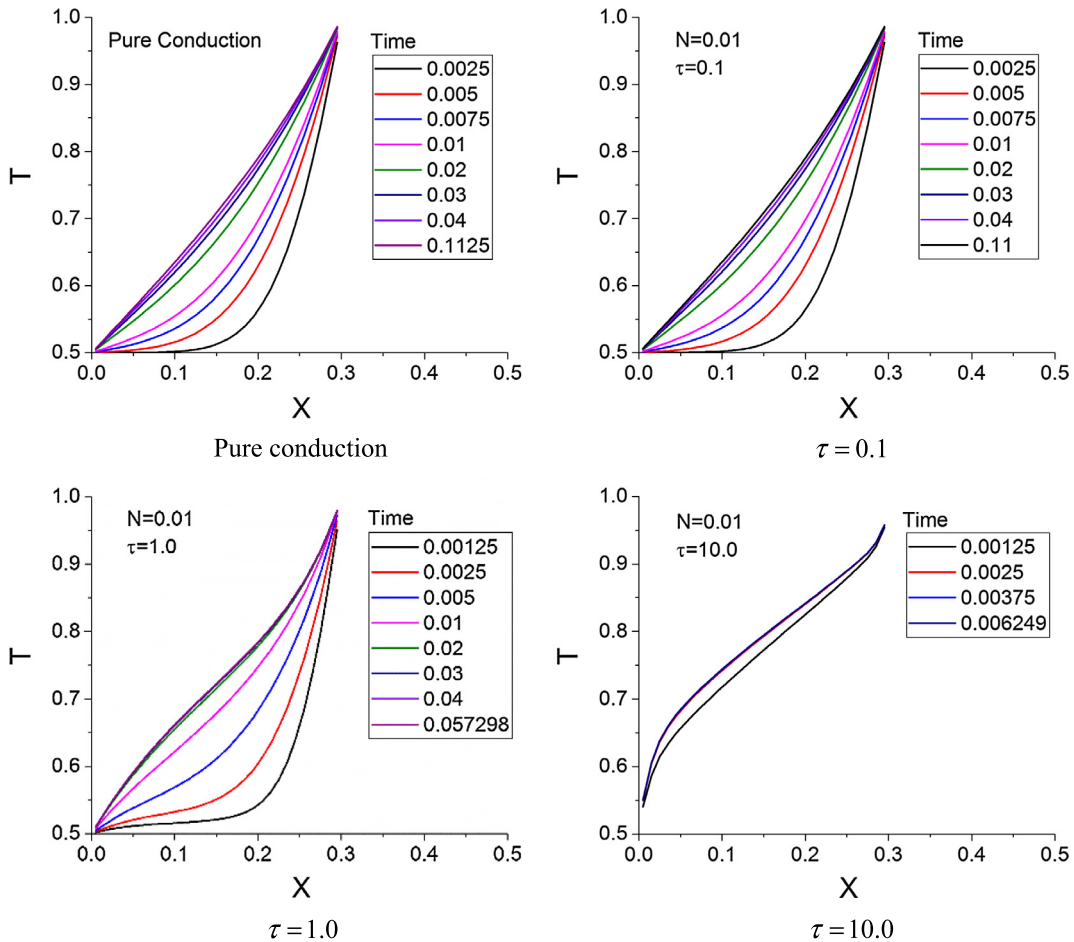


**Fig. 18.** Transient temperature profile along the center line for  $N = 0.01$ .

thickness, indicating that enhanced heat transfer caused by the long-range radiation transfer is negligible compared to the diffusive heat transfer.

### 3.5.2. Transient temperature variations

Fig. 18 shows the temperature evolutions along the horizontal center line for pure conduction and  $N = 0.01$ . Only half of the temperature profile is plotted because it's symmetry to the center line. As discussed earlier, temperature for case with small optical thickness (like 0.1) is almost identical to that of pure conduction case due to negligible effects of radiative heat source to the energy equations. This will also lead to similar temperature evolutions for these two cases, and they take almost the same time to the steady state. When  $\tau = 1.0$ , the temperature evolves faster than the two previous cases. Firstly, temperature of  $\tau = 1.0$  is higher than that of  $\tau = 0.1$ . For example, temperature at  $t = 0.01$  is much larger for case of  $\tau = 1.0$ . Secondly, temperature differences between two consecutive time steps are larger. Because of this, time needed to reach steady state is decreased by half compared to the pure conduction case. When the optical thickness further increases to 10.0, the temperature evolves much faster than the previous cases, and it only need about 0.000625 to reach the steady state. The temperature profile is in highly non-linear distribution with large temperature gradient near the boundaries due to the domination of radiation transfer. As the time scale of the radiative transfer is much faster than that of conduction transfer, its domination over conduction will lead to fast energy transfer and the

establishment of the steady temperature field. This indicates that the competition between conduction and radiation is dependent both on conduction-radiation number and optical thickness.

### 3.5.3. Effects of wall emissivity and scattering on the heat flux

As wall heat flux is important for heat transfer analyses, this section will investigate the effect of wall emissivity and scattering on the conductive, radiative and total heat flux along the cold wall. Only the case of  $N = 0.01$  is considered here, in which radiation dominates over conduction.

Fig. 19 shows the non-dimensional conductive, radiative and total heat flux along the bottom wall for different wall emissivities for  $N = 0.01$ ,  $\tau = 1.0$ . Emissivity of the inner circular wall is fixed to 1.0. As shown in the figure, the conductive heat flux increases with the decrease of the wall emissivity, indicating larger temperature gradient near the wall. The reason for this phenomenon is that more energy will be reflected to the medium from the wall with smaller emissivity. Consequently, wall radiative heat flux will decrease with the decrease of the wall emissivity, as shown in Fig. 19(b). Due to the ray effect, the radiative heat flux is oscillating.

When emissivity is 1.0, the conductive heat flux is in the range of 0–0.08, while the radiative heat flux is much larger, and is in the range of 0.15–0.35. As the radiative heat flux decreases faster than the increase of the conductive heat flux when the emissivity decreases, the total heat flux is smaller for smaller emissivity.

Fig. 20 shows the non-dimensional conductive, radiative and total heat flux along the bottom wall for different scattering albe-

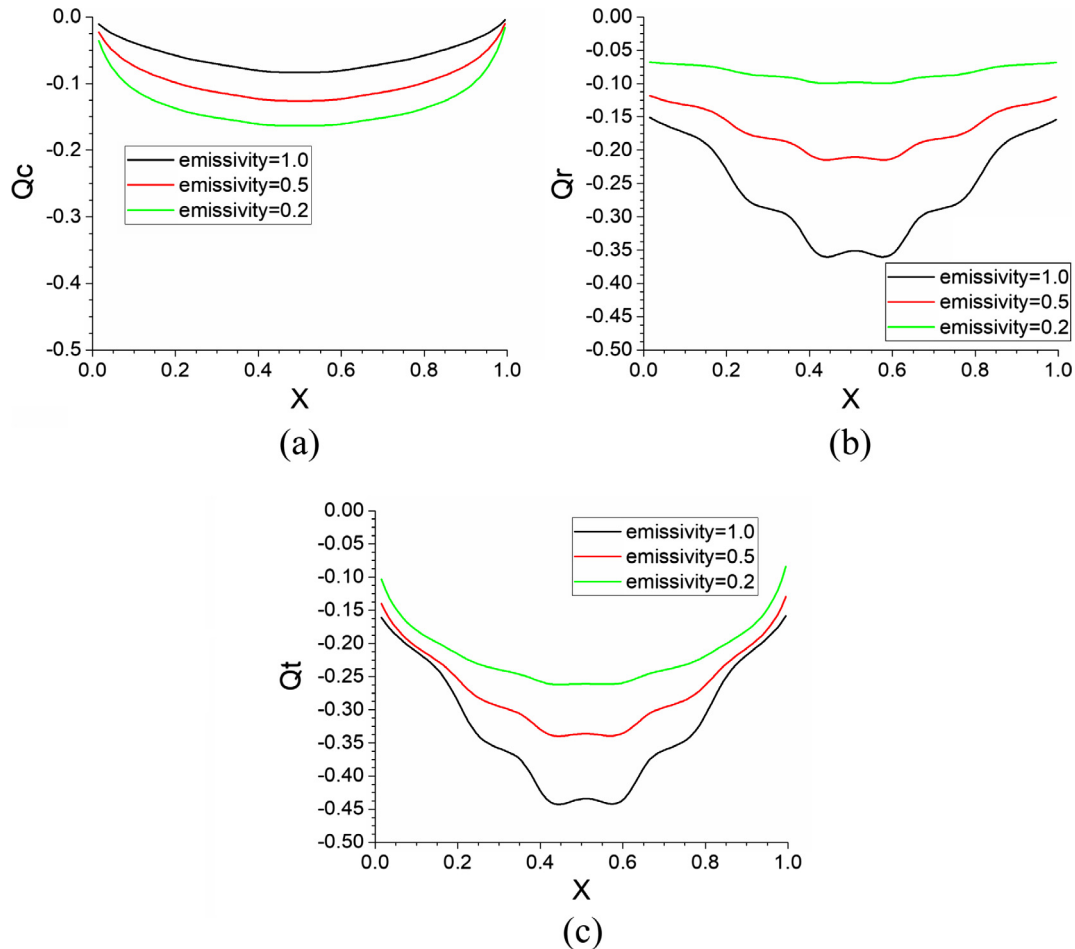


**Fig. 19.** Heat flux along the bottom wall for different emissivities for  $N = 0.01$ ,  $\tau = 1.0$ .

dos for  $N = 0.01$ ,  $\tau = 1.0$ . All wall emissivities are set to 1.0. Isotropic scattering is assumed. As can be seen from Fig. 20(a), the conductive heat flux will increase with the increase of scattering albedo, while the radiative heat flux is almost not affected. Thus, the total heat flux is larger for larger scattering albedo.

#### 4. Conclusions

Lattice Boltzmann method and finite volume method are coupled to solve the combined conduction and radiation heat transfer in irregular geometries for the first time. The LBM is used to solve the energy equation and the FVM is used to solve the radiative transfer equation. Blocked-off method is used in the FVM to enable its capability of treating complex boundary in Cartesian grid systems to incorporate the radiative heat source information into the LBM solver without any additional operations, such as interpolation between different grid systems.

LBM and blocked-off FVM are validated by pure conduction heat transfer problem and pure radiation heat transfer problem in irregular geometries, respectively. Two combined conduction and radiation cases are chosen from existing articles to evaluate the performance of present LBM-FVM. Results of this hybrid method shows good agreement with those in the reference paper. This method has good capabilities in predicting temperature profiles and wall heat flux along straight boundary. We develop a method to obtain the conductive and radiative heat flux along inclined and curved walls, and due to that the complex boundary

is approximated as step-like grids, the heat flux shows an oscillatory behavior.

This hybrid method is also used to solve a combined conduction and radiation heat transfer in a square enclosure with internal circular wall. Results shows that the interaction of conduction and radiation is dependent on conduction-radiation number and optical thickness. Radiation will dominate for small conduction-radiation number with large optical thickness. Increasing the conduction-radiation number or decreasing the optical thickness will lead to domination of the conduction. Additionally, physical time for the system evolving from initial condition to the steady state is dependent on which energy transfer mode is dominating, and it shows that this time is very small for radiation dominating cases while larger for conduction dominating cases. Wall emissivity has an important impact on the wall heat flux. The conductive heat flux increases with the decrease of the emissivity, while the radiative heat flux and total heat flux will decrease for the case of  $N = 0.01$ . Scattering albedo has an obvious influence on the conductive heat flux, while small impact on the radiative heat flux.

The results show that the proposed hybrid solver can solve combined conduction and radiation in irregular geometries, providing a technique to treat complex boundaries in conjugate heat transfer in the framework of LBM.

#### Conflict of interest

No conflict of interest.

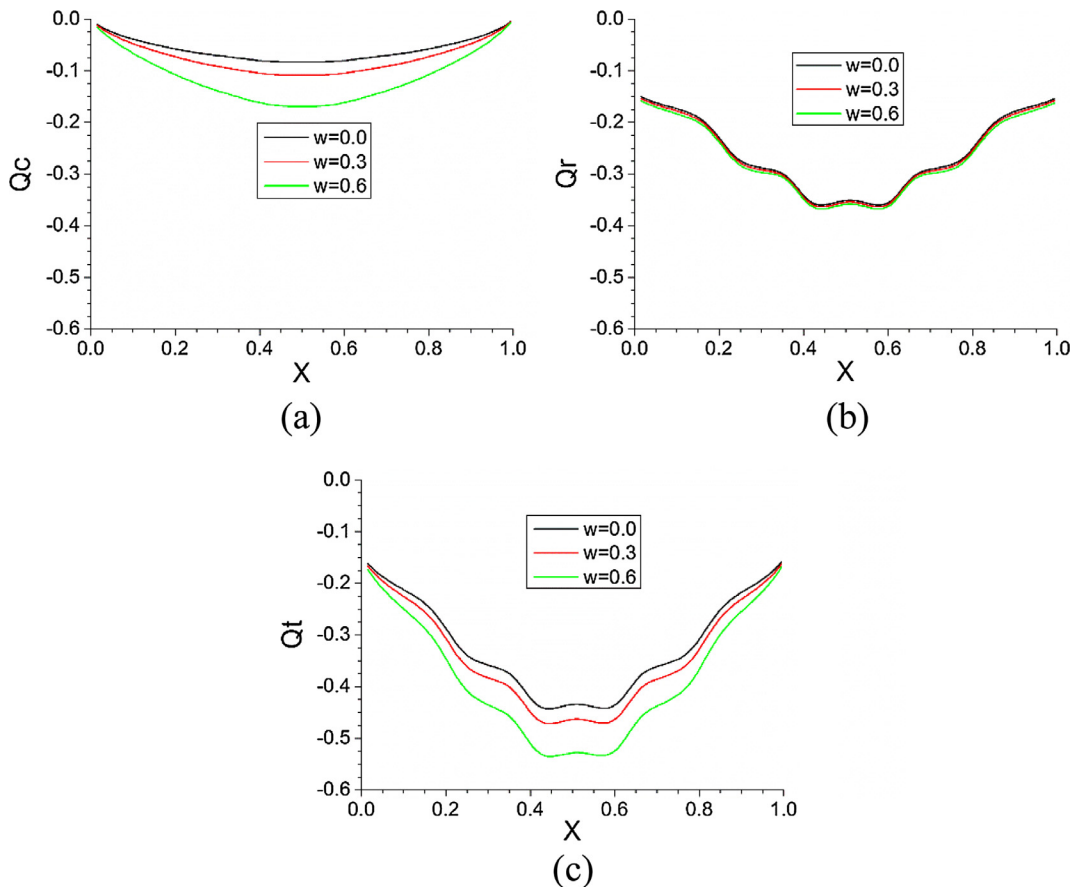


**Fig. 20.** Heat flux along the bottom wall for different scattering albedo for  $N = 0.01$ ,  $\tau = 1.0$ .

## References

- [1] X. He, S. Chen, G.D. Doolen, A novel thermal model for the lattice Boltzmann method in incompressible limit, *J. Comput. Phys.* 146 (1998) 282–300, <https://doi.org/10.1006/jcph.1998.6057>.
- [2] Y. Peng, C. Shu, Y.T. Chew, Simplified thermal lattice Boltzmann model for incompressible thermal flows, *Phys. Rev. E* 68 (2003) 26701, <https://doi.org/10.1103/PhysRevE.68.026701>.
- [3] G.H. Tang, W.Q. Tao, Y.L. He, Simulation of fluid flow and heat transfer in a plane channel using the lattice Boltzmann method, *Int. J. Mod. Phys. B* 17 (2003) 183–187, <https://doi.org/10.1142/S0217979203017485>.
- [4] Q. Li, Y.L. He, Y. Wang, G.H. Tang, An improved thermal lattice Boltzmann model for flows without viscous heat dissipation and compression work, *Int. J. Mod. Phys. C* 19 (2008) 125–150, <https://doi.org/10.1142/S0129183108011978>.
- [5] Y.Y. Yan, Y.Q. Zu, Numerical simulation of heat transfer and fluid flow past a rotating isothermal cylinder-A LBM approach, *Int. J. Heat Mass Transf.* 51 (2008) 2519–2536, <https://doi.org/10.1016/j.ijheatmasstransfer.2007.07.053>.
- [6] A.A. Mohamad, A. Kuzmin, A critical evaluation of force term in lattice Boltzmann method, natural convection problem, *Int. J. Heat Mass Transf.* 53 (2010) 990–996, <https://doi.org/10.1016/j.ijheatmasstransfer.2009.11.014>.
- [7] A.A. Alamyane, A.A. Mohamad, Simulation of forced convection in a channel with extended surfaces by the lattice Boltzmann method, *Comput. Math. with Appl.* 59 (2010) 2421–2430, <https://doi.org/10.1016/j.camwa.2009.08.070>.
- [8] T. Zhang, B. Shi, Z. Guo, Z. Chai, J. Lu, General bounce-back scheme for concentration boundary condition in the lattice-Boltzmann method, *Phys. Rev. E – Stat. Nonlinear, Soft Matter Phys.* 85 (2012) 1–14, <https://doi.org/10.1103/PhysRevE.85.016701>.
- [9] F. Moufekkir, M.A. Moussaoui, A. Mezrhab, H. Naji, D. Lemonnier, Numerical prediction of heat transfer by natural convection and radiation in an enclosure filled with an isotropic scattering medium, *J. Quant. Spectrosc. Radiat. Transf.* 113 (2012) 1689–1704, <https://doi.org/10.1016/j.jqsrt.2012.04.017>.
- [10] K.-H. Lin, C.-C. Liao, S.-Y. Lien, C.-A. Lin, Thermal lattice Boltzmann simulations of natural convection with complex geometry, *Comput. Fluids* 69 (2012) 35–44, <https://doi.org/10.1016/j.compfluid.2012.08.012>.
- [11] R. Khazaeei, S. Mortazavi, M. Ashrafizadeh, Application of a ghost fluid approach for a thermal lattice Boltzmann method, *J. Comput. Phys.* 250 (2013) 126–140, <https://doi.org/10.1016/j.jcp.2013.04.044>.
- [12] Q. Chen, X. Zhang, J. Zhang, Improved treatments for general boundary conditions in the lattice Boltzmann method for convection-diffusion and heat transfer processes, *Phys. Rev. E* 88 (2013) 33304, <https://doi.org/10.1103/PhysRevE.88.033304>.
- [13] Z. Li, M. Yang, Y. Zhang, A coupled lattice Boltzmann and finite volume method for natural convection simulation, *Int. J. Heat Mass Transf.* 70 (2014) 864–874, <https://doi.org/10.1016/j.ijheatmasstransfer.2013.11.077>.
- [14] Q. Chen, X. Zhang, J. Zhang, Numerical simulation of Neumann boundary condition in the thermal lattice Boltzmann model, *Int. J. Mod. Phys. C* 25 (2014) 1–13, <https://doi.org/10.1142/S0129183114500272>.
- [15] Q. Chen, X.B. Zhang, Q. Li, X.S. Jiang, H.P. Zhou, Study of three-dimensional electro-osmotic flow with curved boundary via lattice Boltzmann method, *Int. J. Mod. Phys. C* 27 (2016) 1650063, <https://doi.org/10.1142/S0129183116500637>.
- [16] Q. Li, K.H. Luo, Q.J. Kang, Y.L. He, Q. Chen, Q. Liu, Lattice Boltzmann methods for multiphase flow and phase-change heat transfer, *Prog. Energy Combust. Sci.* 52 (2016) 62–105, <https://doi.org/10.1016/j.pecs.2015.10.001>.
- [17] Y. Sun, X. Zhang, Analysis of transient conduction and radiation problems using the lattice Boltzmann and discrete ordinates methods, *Numer. Heat Transf. Part A Appl. An Int. J. Comput. Methodol.* 68 (2015) 619–637, <https://doi.org/10.1080/10407782.2014.994406>.
- [18] B. Mondal, S.C. Mishra, Application of the lattice Boltzmann method and the discrete ordinates method for solving transient conduction and radiation heat transfer problems, *Numer. Heat Transf. Part A Appl.* 52 (2007) 757–775.
- [19] S.C. Mishra, H.K. Roy, Solving transient conduction and radiation heat transfer problems using the lattice Boltzmann method and the finite volume method, *J. Comput. Phys.* 223 (2007) 89–107, <https://doi.org/10.1016/j.jcp.2006.08.021>.
- [20] Y. Sun, X. Zhang, Analysis of transient conduction and radiation problems using lattice Boltzmann and finite volume methods, *Int. J. Heat Mass Transf.* 97 (2016) 611–617, <https://doi.org/10.1016/j.ijheatmasstransfer.2016.01.074>.
- [21] R. Chaabane, F. Askri, S. Ben Nasrallah, Application of the lattice Boltzmann method to transient conduction and radiation heat transfer in cylindrical media, *J. Quant. Spectrosc. Radiat. Transf.* 112 (2011) 2013–2027, <https://doi.org/10.1016/j.jqsrt.2011.04.002>.
- [22] S.C. Mishra, H. Poonia, A.K. Das, P. Asinari, R. Borchiellini, Analysis of conduction-radiation heat transfer in a 2D enclosure using the lattice Boltzmann method, *Numer. Heat Transf. Part A Appl.* 66 (2014) 669–688.
- [23] F.-J. Yao, K. Luo, H.-L. Yi, M. Xie, Analysis of melting with natural convection and volumetric radiation using lattice Boltzmann method, *Int. J. Heat Mass Transf.*

- Transf. 112 (2017) 413–426, <https://doi.org/10.1016/j.ijheatmasstransfer.2017.04.136>.
- [24] F. Bouzgarrou, F. Askri, H. Belhaj Ali, S. Ben Nasrallah, Analyses of unsteady conduction-radiation heat transfer using unstructured Lattice Boltzmann method, Int. J. Therm. Sci. 116 (2017) 287–309, <https://doi.org/10.1016/j.ijthermalsci.2017.03.002>.
- [25] M.Y. Kim, S.W. Baek, J.H. Park, Unstructured finite-volume method for radiative heat transfer in a complex two-dimensional geometry with obstacles, Numer. Heat Transf. Part B Fundam. 39 (2001) 617–635, <https://doi.org/10.1080/10407790152034854>.
- [26] M. Sakami, A. Charette, Application of a modified discrete ordinates method to two-dimensional enclosures of irregular geometry, J. Quant. Spectrosc. Radiat. Transf. 64 (2000) 275–298, [https://doi.org/10.1016/S0022-4073\(99\)00100-4](https://doi.org/10.1016/S0022-4073(99)00100-4).
- [27] F. Asllanaj, V. Feldheim, P. Lybaert, Solution of radiative heat transfer in 2-D geometries by a modified finite-volume method based on a cell vertex scheme using unstructured triangular meshes, Numer. Heat Transf. Part B Fundam. 51 (2007) 97–119, <https://doi.org/10.1080/10407790600762805>.
- [28] M.Y. Kim, S.W. Baek, S.I. Park, Evaluation of the finite-volume solutions of radiative heat transfer in a complex two-dimensional enclosure with unstructured polygonal meshes, Numer. Heat Transf. Part B Fundam. 54 (2008) 116–137, <https://doi.org/10.1080/10407790802154215>.
- [29] M. Sakami, A. Charette, Application of the discrete ordinates method to combined conductive and radiative heat transfer in a two-dimensional complex geometry, J. Quant. Spectrosc. Radiat. Transf. 56 (1996) 517–533.
- [30] L.M. Ruan, M. Xie, H. Qi, W. An, H.P. Tan, Development of a finite element model for coupled radiative and conductive heat transfer in participating media, J. Quant. Spectrosc. Radiat. Transf. 102 (2006) 190–202, <https://doi.org/10.1016/j.jqsrt.2006.02.070>.
- [31] N. Aouled-Dlala, T. Sghaier, E. Seddiki, Numerical solution of radiative and conductive heat transfer in concentric spherical and cylindrical media, J. Quant. Spectrosc. Radiat. Transf. 107 (2007) 443–457, <https://doi.org/10.1016/j.jqsrt.2007.02.012>.
- [32] Y. Sun, B. Li, Spectral collocation method for transient conduction-radiation heat transfer, J. Thermophys. Heat Transf. 24 (2010) 823–832, <https://doi.org/10.2514/1.43400>.
- [33] B. Li, Y. Sun, D. Zhang, Chebyshev collocation spectral methods for coupled radiation and conduction in a concentric spherical participating medium, J. Heat Transfer. 131 (2009) 62701, <https://doi.org/10.1115/1.3090617>.
- [34] Y. Sun, J. Ma, B. Li, Z. Guo, Predication of nonlinear heat transfer in a convective-radiative fin with temperature-dependent properties by the collocation spectral method, Numer. Heat Transf. Part B Fundam. 69 (2016) 68–83, <https://doi.org/10.1080/10407782.2015.1081043>.
- [35] J. Ma, Y. Sun, B. Li, H. Chen, Spectral collocation method for radiative-conductive porous fin with temperature dependent properties, Energy Convers. Manage. 111 (2016) 279–288, <https://doi.org/10.1016/j.enconman.2015.12.054>.
- [36] J. Ma, Y. Sun, B. Li, Spectral collocation method for transient thermal analysis of coupled conductive, convective and radiative heat transfer in the moving plate with temperature dependent properties and heat generation, Int. J. Heat Mass Transf. 114 (2017) 469–482, <https://doi.org/10.1016/j.ijheatmasstransfer.2017.06.082>.
- [37] Y. Zhang, Y. Ma, H. Yi, H. Tan, Natural element method for solving radiative transfer with or without conduction in three-dimensional complex geometries, J. Quant. Spectrosc. Radiat. Transf. 129 (2013) 118–130.
- [38] Y. Zhang, H. Yi, H. Tan, Natural element method analysis for coupled radiative and conductive heat transfer in semitransparent medium with irregular geometries, Int. J. Therm. Sci. 76 (2014) 30–42, <https://doi.org/10.1016/j.ijthermalsci.2013.08.013>.
- [39] K. Luo, H. Yi, H. Tan, Eccentricity effect on bifurcation and dual solutions in transient natural convection in a horizontal annulus, Int. J. Therm. Sci. 89 (2015) 283–293, <https://doi.org/10.1016/j.ijthermalsci.2014.11.020>.
- [40] K. Luo, H. Yi, H. Tan, Coupled radiation and mixed convection in an eccentric annulus using the hybrid strategy of lattice boltzmann-meshless method, Numer. Heat Transf. Part B Fundam. 66 (2014) 243–267, <https://doi.org/10.1080/10407790.2014.915668>.
- [41] J.C. Choi, H.O.S. Lee, S.V. Patankar, Treatment of irregular geometries using a Cartesian coordinates finite-volume radiation heat transfer procedure, Numer. Heat Transf. Part B Fundam. 26 (1994) 225–235, <https://doi.org/10.1080/10407799408914927>.
- [42] D. Young Byun, S. Wook Baek, M. Young Kim, Investigation of radiative heat transfer in complex geometries using blocked-off, multiblock, and embedded boundary treatments, Numer. Heat Transf. Part A Appl. 43 (2003) 807–825, <https://doi.org/10.1080/713838148>.
- [43] C. Aghanjafi, A. Abjadpour, Discrete ordinates method applied to radiative transfer equation in complex geometries meshed by structured and unstructured grids, J. Brazilian Soc. Mech. Sci. Eng. (2015), <https://doi.org/10.1007/s40430-015-0397-2>.
- [44] G. Kamel, B.M. Naceur, M. Rachid, S. Rachid, Formulation and testing of the FTn finite volume method for radiation in 3-D complex inhomogeneous participating media, J. Quant. Spectrosc. Radiat. Transf. 98 (2006) 425–445, <https://doi.org/10.1016/j.jqsrt.2005.07.001>.
- [45] P. Talukdar, Radiative heat transfer for irregular geometries with the collapsed dimension method, Int. J. Therm. Sci. 45 (2006) 103–109, <https://doi.org/10.1016/j.ijthermalsci.2005.06.006>.
- [46] P. Talukdar, Discrete transfer method with the concept of blocked-off region for irregular geometries, J. Quant. Spectrosc. Radiat. Transf. 98 (2006) 238–248, <https://doi.org/10.1016/j.jqsrt.2005.05.087>.
- [47] H. Amiri, S.H. Mansouri, A. Safavinejad, Combined conductive and radiative heat transfer in an anisotropic scattering participating medium with irregular geometries, Int. J. Therm. Sci. 49 (2010) 492–503, <https://doi.org/10.1016/j.ijthermalsci.2009.10.005>.
- [48] H. Amiri, S.H. Mansouri, P.J. Coelho, Application of the modified discrete ordinates method with the concept of blocked-off region to irregular geometries, Int. J. Therm. Sci. 50 (2011) 515–524, <https://doi.org/10.1016/j.ijthermalsci.2010.10.012>.
- [49] P. Talukdar, M.A.A. Mendes, R.K. Parida, D. Trimis, S. Ray, Modelling of conduction-radiation in a porous medium with blocked-off region approach, Int. J. Therm. Sci. 72 (2013) 102–114, <https://doi.org/10.1016/j.ijthermalsci.2013.04.027>.
- [50] V.M. Patel, P. Talukdar, Evaluation of radiative properties of a representative foam structure using blocked-off region approach integrated with finite volume method, Int. J. Therm. Sci. 108 (2016) 89–99, <https://doi.org/10.1016/j.ijthermalsci.2016.05.003>.
- [51] M. Zabihi, K. Lari, H. Amiri, Coupled radiative-conductive heat transfer problems in complex geometries using embedded boundary method, J. Brazilian Soc. Mech. Sci. Eng. 39 (2017) 2847–2864, <https://doi.org/10.1007/s40430-017-0729-5>.